공학석사학위논문

불확실성을 고려한 고고도 과학 기구의 궤적 예측 연구

Numerical Prediction of Scientific Balloon Trajectories While Considering Various Uncertainties

2017 년 2 월

서울대학교 대학원

기계항공공학부

이 용 선

초 록

고고도 과학 기구(氣球)는 기상 환경의 영향을 크게 받는 특성으로 인해 한번 발사한 후에는 고도 제어를 제외하고는 움직임의 제어가 불가능하다. 따라서 기구 운용으로 인한 사고 발생을 막기 위해 과학 기구의 발사 전에 기구의 궤적을 정확하게 예측하여 운용 가능 여부를 확인하는 것이 중요하다. 기존 연구들의 기구 궤적 예측 결과는 기구 운용 및 궤적 예측 과정에서 발생하는 불확실성들을 고려하지 못했으므로 실제 기구 비행 궤적과 정확히 일치하지 않는 문제가 있었다. 본 연구에서는 실제 기구 운용에 유용한 궤적 예측 결과를 얻기 위해 불확실성을 고려한 확률론적인 방법의 사용을 제안한다. 기구의 형상 설계, 기구의 열역학 및 동역학적 특성에 관한 연구를 진행하여 고고도 과학 기구의 궤적 예측 시뮬레이션 프로그램을 개발하였고, 몬테카를로 시뮬레이션을 이용하여 기구 운용 및 궤적 예측 상의 불확실성을 고려한 비행 궤적 예측 시뮬레이션 결과를 도출하였다. 각 불확실성이 기구 궤적에 미치는 영향을 알아보기 위해 민감도 조사를 진행한 결과, 예측 오류에 가장 큰 영향을 미치는 것은 발사 전 기구에 주입되는 헬륨의 질량, 즉 기구 운용 상의 불확실성인 것으로 나타났다.

주요어 : 고고도 과학 기구, 궤적 예측, 불확실성, 몬테카를로 시뮬레이션

학 번 : 2015-20786

ABSTRACT

Numerical Prediction of Scientific Balloon Trajectories While Considering Various Uncertainties

Yongseon Lee
Mechanical and Aerospace Engineering
The Graduate School
Seoul National University

Before launching a scientific balloon, one needs to precisely predict its trajectory to avoid any possible accidents, as there are no means to control the horizontal motion of the balloon once it is launched. Although earlier studies developed simulation programs that predicted the trajectory of a scientific balloon with reasonable accuracy, the simulated results were hardly the same as the actual balloon flight because there existed uncertainties in balloon trajectory prediction. To address the difference between the predicted and actual flight trajectories, the prediction should be probabilistic, which means the uncertainties involved in the calculation should be taken into account. In the present work, a numerical simulation program is developed to predict the trajectories of a balloon, while considering various uncertainties, with the use

of a Monte Carlo simulation. Sensitivity studies are performed to identify the most dominant uncertainty parameter in the distribution of landing points of the balloon flight. Operational uncertainty represented by the amount of buoyant gas is shown to be the most significant source of the prediction error, although it can be overcome by controlling the amount of lifting gas during the actual flight.

keywords : Scientific Balloon, High Altitude Balloon, Uncertainty, Trajectory Prediction, Monte Carlo Simulation

***Student Number* : 2015-20786**

LIST

LIST OF FIGURES

I. Introduction

A scientific balloon is a stratospheric balloon that is used for scientific and engineering research. It can fly as high as 40 km with payloads as heavy as several tons. In general, a scientific balloon consists of an envelope, a parachute, and a payload. The envelope includes an exhaust valve and a tear panel. The exhaust valve releases the lifting gas to lower the altitude of the balloon, and the tear panel rips the balloon film when the flight is terminated. The parachute slows the freefall of the payload after flight termination so that the payload can be retrieved without damage. The payload contains mission instruments, equipment for telecommunication with the ground facility, and ballast. When the balloon needs to accelerate its ascending speed, the ballast is dropped to lighten the balloon system. The payload usually contains costly equipment, so it needs to be retrieved after the flight is terminated. Scientific ballooning procedures include the launching of a scientific balloon, the mission flight of the balloon, separating the envelope and the parachute, and retrieving the mission payload. Figure 1 schematically shows these procedures.

Compared to rocket and ground-test facilities, the scientific balloon can be a cost-efficient platform to carry out astrophysical experiments in the near-space environment. Balloon-borne astrophysical studies have yielded important results over the past few decades [1]. The use of scientific balloons has expanded outside academic studies in recent years. In 2007, the Italian Aerospace Research Centre (known as CIRA) conducted a dropped transonic flight test of an unmanned space vehicle using a scientific balloon [2]. In 2009,

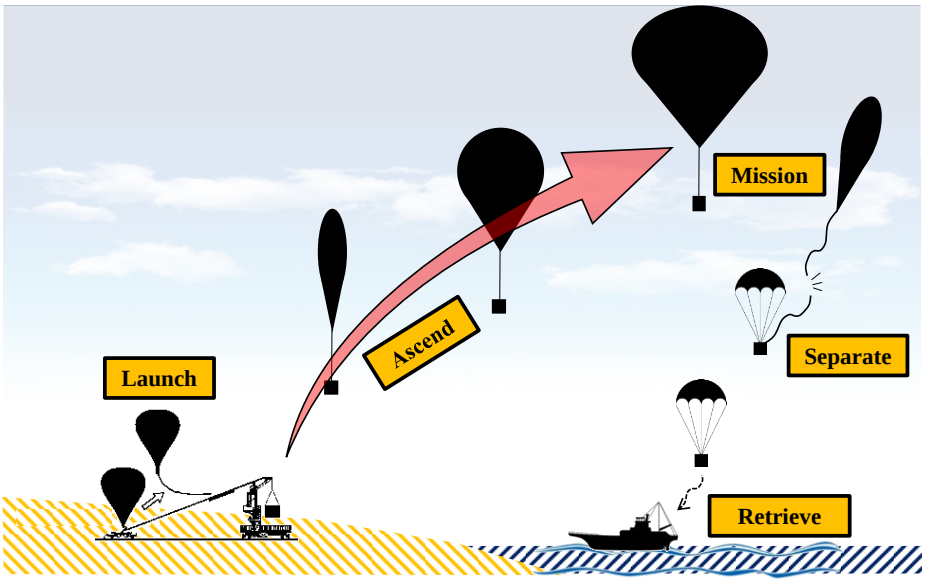

Fig. 1 Schematic diagram of scientific ballooning.

Japan carried out a balloon drop test of a flexible aeroshell and acquired data on the behavior of an inflatable torus attached to the aeroshell [3]. In 2013, Google announced the innovative Project Loon, which aims to provide balloon-powered Internet service in rural and remote areas using a multitude of high-altitude balloons [4]. In 2014, NASA conducted a successful balloon flight mission to demonstrate low-density supersonic decelerator technology [5].

Flying a scientific balloon demands some preparation, which includes studying the balloon's shape and design, as well as acquiring skills in manufacturing, launching, and retrieving the balloon. When a scientific balloon is manufactured and ready to fly, it is necessary to precisely predict the trajectory of the balloon to prevent any unexpected accidents because there are no means to control the horizontal motion during the flight. The separated payload can be dropped on a populated area, damaging houses or blocking

roads; it can even penetrate the border of neighboring foreign countries, causing diplomatic issues. The situation becomes even worse for a small country such as the Republic of Korea, where the territory is extremely narrow and a balloon is apt to cross the border. Aside from avoiding accidents, there are additional benefits to accurate prediction, such as reducing the cost of payload retrieval on the sea.

Several simulation programs for predicting balloon trajectories have already been made and have achieved reasonable accuracy [6–9]. Although past studies have achieved a useful level of accuracy in predicting a balloon's movements, the simulation results could hardly be the same as the actual balloon flight because there exist uncertainties in balloon trajectory prediction. Therefore, the trajectory should be predicted in a probabilistic manner, and the uncertainties involved in the calculation of the trajectory should be taken into account to improve the prediction. Palumbo et al. took into account the uncertainties of wind, ambient air temperature, and pressure forecasts, as well as the mass of buoyant gas transferred to the balloon [10]. Although this methodology was able to produce a probabilistic dispersion area without Monte Carlo analysis, the relative sensitivity of each uncertainty was not shown individually. Sóbester et al. introduced a process that generates Monte Carlo ensembles of simulated trajectories of a meteorological balloon [11]. To address the incomplete understanding of the drag of balloons, they proposed a novel stochastic drag model based on empirical data derived from a number of radiosonde flights. The Monte Carlo predictor is available online and can be run for free, but the simulation deals only with a meteorological balloon. Dai et al. discussed the influence of film radiation properties and clouds on the thermal behavior of a

high-altitude balloon [12]. In their work, the trajectory variation with respect to the change in the balloon's thermal behavior was not provided. Zhang and Liu revealed the influences of initial launch conditions on the flight performance of a high-altitude balloon [13]. These influences were shown in the form of the rate of climb, but they failed to discuss how a change in the rate of climb affected the balloon's trajectory.

The uncertainties in balloon trajectory prediction can be classified into four categories: operational uncertainty, uncertainty in the prediction model, environmental uncertainty, and manufactural uncertainty. The aforementioned works mostly focused on operational and environmental uncertainties; discussions on prediction model and manufactural uncertainties are relatively rare. Previous works investigating the effect of manufactural uncertainty on balloon trajectory can scarcely be found, even though such an uncertainty should have an effect. For instance, the balloon would not reach its aimed altitude and accomplish its mission if the actual volume of the envelope was different from the manufacturer's stated design, so manufactural uncertainty has to be integrated in the uncertainty analysis.

Furthermore, the previous works usually investigated the influence of each uncertainty or integrated the uncertainties in the trajectory prediction and then discussed the results without comparing the individual influence of each uncertainty. A sensitivity study of each uncertainty, however, needs to be made to clarify the uncertainty that dominates the error between the actual and the predicted trajectories so that the uncertainty is thoroughly addressed when scheduling the launch of a scientific balloon. If the dominant uncertainty is clarified and one pays special attention to that uncertainty source, the difference

between the predicted trajectory and the actual flight trajectory could be minimized.

Therefore, in the present work, a flight simulation program is developed to numerically predict the trajectory of a scientific balloon while considering various uncertainties. The uncertainties include operational uncertainty, uncertainty in the prediction model, environmental uncertainty, and manufactural uncertainty. For the operational uncertainty, the amount of lifting gas injected to launch a balloon is considered by varying the free lift ratio. The drag coefficient of the balloon envelope represents the uncertainty in the prediction model, and wind profile data were selected for the environmental uncertainty. For the manufactural uncertainty, the volume of the manufactured envelope is considered. The uncertainty analyses were conducted with the use of a Monte Carlo simulation. The features of the present research are twofold:

1) Manufactural uncertainty, along with other uncertainties, is considered.

2) The influences of uncertainties on the balloon's trajectory are discussed.

The present work aims to investigate the impact manufactural error in the envelope's volume has on the balloon's flight trajectory so that the balloon manufacturer can decide the error tolerance within which the balloon flight can fulfill its mission. Moreover, the present work aims to determine the effect of each uncertainty on the balloon's trajectory to instruct the balloon flight planner on how to address the dominant uncertainty parameter.

II. Simulation program development and its validation

A scientific balloon is a lighter-than-air vehicle that uses the buoyant force of a lifting gas for flight. Because the buoyant force determines the ascending speed of the balloon, the force should be calculated correctly throughout the balloon's flight. Another important force acting on the balloon is the drag force. The drag force is related to both the horizontal and vertical motion of a scientific balloon. The drag force acts in the opposite direction of the balloon's movement, so calculating the force is important for precisely predicting the ascending rate of the balloon. For horizontal motion, the drag force is the only source of motion, but one does not need to calculate the force in this situation—the balloon velocity quickly becomes the same as the wind velocity. To calculate the buoyant and drag forces acting on a scientific balloon, it is necessary to know the volume and the surface area of the balloon. The volume and the surface area, however, vary according to the shape of the envelope and the temperature of the lifting gas. The simulation program used in the present work determines the shape of the balloon when the flight mission is given, and it predicts the flight trajectory with an appropriate thermal model to calculate the temperature of the lifting gas.

A. Design of the Balloon

Scientific balloons can be classified into two categories: zero-pressure balloons, which have venting ducts so that the pressure inside the envelope is the same as the atmospheric pressure; and super-pressure balloons, which are completely sealed so the gas cannot leak out of the balloon envelope. Zero-pressure balloons are relatively easy to manufacture and operate, and their flight duration is relatively short (usually several hours); whereas super-pressure balloons can fly for a number of days but require a much more sophisticated manufacturing technology. In this paper, the zero-pressure balloon category is chosen as the target of the trajectory prediction because the mission flight is planned to terminate several hours after the launch.

To design a zero-pressure balloon, the design procedure for a Σ-shape natural shape balloon, introduced in Yajima et al.'s work [14], was followed. The specific procedure to design a Σ-shape natural shape balloon is described in Appendix A. Following the procedure to solve the force equilibrium equations, ordinary differential equations (ODEs) concerned with the relationship among the tension $\tilde{T}_\theta$, weight Σ_e, and buoyant force b_g of the balloon film can be derived as follows:

$$\tilde{r}\tilde{T}_\theta \frac{\mathrm{d}\theta}{\mathrm{d}\tilde{s}} = -k\Sigma_e \tilde{r} \frac{\mathrm{d}\tilde{r}}{\mathrm{d}\tilde{s}} - (\tilde{z} - \tilde{z}_b)\tilde{r}$$

$$\frac{\mathrm{d}(\tilde{r}\tilde{T}_\theta)}{\mathrm{d}\tilde{s}} = k\Sigma_e \tilde{r} \frac{\mathrm{d}\tilde{z}}{\mathrm{d}\tilde{s}}$$

$$\frac{\mathrm{d}\tilde{r}}{\mathrm{d}\tilde{s}} = \sin\theta, \quad \frac{\mathrm{d}\tilde{z}}{\mathrm{d}\tilde{s}} = \cos\theta, \quad \frac{\mathrm{d}\tilde{S}}{\mathrm{d}\tilde{s}} = 2\pi\tilde{r}, \quad \frac{\mathrm{d}\tilde{V}}{\mathrm{d}\tilde{s}} = \pi\tilde{r}^2 \frac{\mathrm{d}\tilde{z}}{\mathrm{d}\tilde{s}}$$

$$\text{where } k = (2\pi)^{-(1/3)}, \quad \tilde{T}_\theta = \frac{T_\theta}{b_g \lambda^2}, \quad \Sigma_e = \frac{w_e g}{k b_g \lambda} \tag{1}$$

The fully inflated shape of a Σ-shape natural shape balloon can be achieved when the ODEs in Eq. (1) are solved numerically with the following initial conditions:

$$\tilde{r} = \tilde{z} = \tilde{S} = \tilde{V} = 0, \quad \tilde{r}\tilde{T}_\theta = \frac{1}{2\pi\cos\theta_0} \tag{2}$$

When solving Eq. (1) numerically, the length of the film l_s and the initial angle θ_0 in Eq. (2) are determined by a shooting method. After the balloon shape at the maximum altitude is fixed, the maximum volume as well as the surface area and the weight of the envelope of the balloon are obtained. In the procedure, the undefined parameters are the target altitude, the suspending load on the balloon, and the density and thickness of the polyethylene film, which are determined by the mission profile.

B. Equations of Motion

The motion of a scientific balloon occurs in the vertical and horizontal directions. For the vertical motion of the balloon, in which its altitude changes, the total weight of the balloon system, the buoyant force, and the drag force of the balloon are the main components that should be noted when calculating the motion. When $\boldsymbol{V}_x$, $\boldsymbol{V}_y$, and $\boldsymbol{V}_z$ and $\boldsymbol{u}_{\text{wind}}$, $\boldsymbol{v}_{\text{wind}}$, and $\boldsymbol{w}_{\text{wind}}$ represent the absolute velocity components of the balloon and the wind, respectively, the relative velocity components and the magnitude of the relative velocity of the balloon can be calculated as follows:

$$\begin{aligned}
\boldsymbol{V}_{\text{relx}} &= \boldsymbol{u}_{\text{wind}} - \boldsymbol{V}_x \\
\boldsymbol{V}_{\text{rely}} &= \boldsymbol{v}_{\text{wind}} - \boldsymbol{V}_y \\
\boldsymbol{V}_{\text{relz}} &= \boldsymbol{w}_{\text{wind}} - \boldsymbol{V}_z \\
|\boldsymbol{V}_{\text{rel}}| &= (\boldsymbol{V}_{\text{relx}}^2 + \boldsymbol{V}_{\text{rely}}^2 + \boldsymbol{V}_{\text{relz}}^2)^{1/2}
\end{aligned} \tag{3}$$

Then, the magnitude of the drag force and its components are determined with the following equations:

$$\begin{aligned}
\text{Drag} &= \frac{1}{2} \cdot \rho_{\text{air}} \cdot \boldsymbol{V}_{\text{rel}}^2 \cdot C_d \cdot A_{\text{top}} \\
\text{Drag}_z &= \text{Drag} \cdot \frac{|\boldsymbol{V}_{\text{relz}}|}{|\boldsymbol{V}_{\text{rel}}|}
\end{aligned} \tag{4}$$

where the reference area $A_{\text{top}} = \pi r_{\text{max}}^2$ is the top projected area. The value of the buoyant force can be defined using the following equation:

$$F_{\text{buoyant}} = \rho_{air} \cdot \text{Volume} \cdot g \tag{5}$$

For the horizontal motion of the balloon, in which its latitude or longitude changes, only the drag force drives the motion, unless there is a source to

control the balloon's motion:

$$\begin{aligned} \text{Drag}_y &= \text{Drag} \cdot \frac{|\boldsymbol{V}_{\text{rely}}|}{|\boldsymbol{V}_{\text{rel}}|} \\ \text{Drag}_x &= \text{Drag} \cdot \frac{|\boldsymbol{V}_{\text{relx}}|}{|\boldsymbol{V}_{\text{rel}}|} \end{aligned} \tag{6}$$

In the motion equations, the mass of air that is dragged along with the motion of the balloon should be considered as well. Therefore, m_{virtual} is introduced using the following equation:

$$m_{\text{virtual}} = m_{\text{total}} + C_{\text{virtual}} \cdot \rho_{\text{air}} \cdot \text{Volume} \tag{7}$$

and the value of 0.37 is used for the virtual mass coefficient C_{virtual} in this study. Finally, the equations of motion can be written as follows:

$$\begin{aligned} m_{\text{virtual}} \ddot{x} &= \text{Drag}_x \\ m_{\text{virtual}} \ddot{y} &= \text{Drag}_y \\ m_{\text{virtual}} \ddot{z} &= F_{\text{buoyant}} - m_{\text{total}} \cdot g + \text{Drag}_z \end{aligned} \tag{8}$$

C. Thermal Model

When predicting the trajectory of a scientific balloon, the temperature of the lifting gas in the balloon should be predicted accurately because it critically affects the balloon's motion. As shown in Eq. (8), the motion of the balloon in the horizontal direction is solely dependent on the drag, and the drag is a function of the temperature of the gas, which determines the volume and surface area of the balloon. The volume of the buoyant gas, which is assumed to be the same as the volume of the envelope, is calculated with the ideal gas equation $\text{Volume} = (m_{\text{gas}} R_{\text{gas}} T_{\text{gas}} / P)$ during the flight. In regard to vertical motion, it is even more important to calculate the temperature of the lifting gas precisely. Unlike horizontal motion, the rate of climb is affected by the buoyant force, which the volume of the envelope is directly related to. Moreover, the error in predicting the rate-of-climb results in a significant difference between the position of the simulated trajectory and the actual one because the wind direction and velocity vary along the balloon's altitude.

Figure 2 illustrates the forces acting on a balloon and the heat transfer into and out of a balloon. In this study, the lifting gas is assumed to interact only with the film of the balloon because the helium gas is transparent and the effects of radiative heat transfer are negligible. Accordingly, the following equation can be used to obtain the temperature of the lifting gas:

$$\frac{\mathrm{d}T_{\text{gas}}}{\mathrm{d}t} = \frac{Q_{\text{convInt}}}{c_v \cdot m_{gas}} + (\gamma - 1) \cdot \frac{T_{\text{gas}}}{\rho_{\text{gas}}} \cdot \frac{\mathrm{d}\rho_{\text{gas}}}{\mathrm{d}t} \tag{9}$$

In Eq. (9), the subscript convInt refers to internal convection that occurs inside the balloon film. The mass, temperature, and density of the buoyant gas are

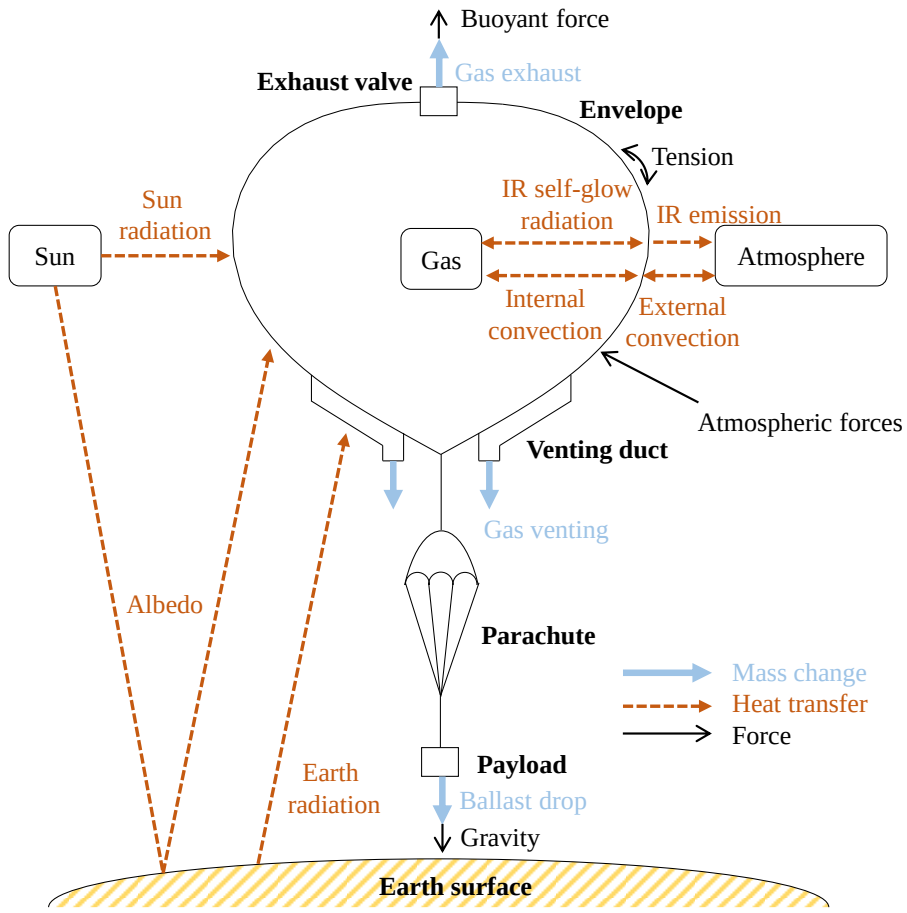

Fig. 2 Forces acting on a balloon and heat transfer into and out of a balloon [14].

represented by m_{gas}, T_{gas}, and ρ_{gas}, respectively.

The specific heat at a constant volume of the lifting gas is denoted by c_v. If there exists no interaction between the lifting gas and the film, Eq. (9) depicts the adiabatic temperature change of the gas.

To calculate the temperature of the envelope film, additional terms of the heat fluxes are added:

$$\frac{\mathrm{d}T_{\mathrm{film}}}{\mathrm{d}t} = \frac{Q_{\mathrm{sun}} + Q_{\mathrm{albedo}} + Q_{\mathrm{IRplanet}} + Q_{\mathrm{IRfilm}} + Q_{\mathrm{convExt}} - Q_{\mathrm{convInt}} - Q_{\mathrm{IRout}}}{c_f \cdot m_{\mathrm{balloon}}} \quad (10)$$

In Eq. (10), the specific heat of the film material is denoted by c_f. Q_{sun} is the absorbed direct solar heat flux, Q_{albedo} is the absorbed albedo heat flux, Q_{IRplanet} is the absorbed planetary IR heat flux, Q_{convExt} is the convectional heat flux between the film and the atmosphere, Q_{convInt} is the convectional heat flux between the film and the lifting gas, and Q_{IRout} is the emitted IR energy from the balloon film. The equations for calculating each term are described in Appendix B. The values used in the calculation were taken from Farley's work [6].

D. Code Validation

The straightforward way to validate the developed code would be to compare the simulation results to real flight data, but it is not as simple as expected to properly use the actual flight data. To use the actual flight data for the validation of the prediction code, 1) the input parameters to predict the flight trajectory of the scientific balloon should be well specified, and 2) the atmospheric data obtained during the flight should be minutely logged. Unfortunately, most flight data satisfy neither condition.

To verify the trajectory simulation program, the simulation results were compared with those of NASA's Scientific Balloon Analysis Model (known as SINBAD) [7] and Palumbo et al.'s code [8]. The simulation input data used for the comparison can be found in another Palumbo work [15]. The reference balloon flight missions were the 2003 Huygens Atmospheric Structure Instrument (HASI) and the Atmospheric Reentry Demonstrator (ARD) capsule. The simulation results are shown in Fig. 3. For both cases, ACHAB used varying drag coefficients given as a function of the Froude number *Fr* and the Reynolds number *Re*. The simulation results were shown to follow the actual flight data. The following relationship was used for the drag coefficient:

$$C_d = 0.2\frac{k}{Fr}\cdot\left(\frac{k_1}{Re}+k_2 Re\right)\frac{A_{top}}{A_{top0}}, \quad k=\frac{K_{\mathrm{CD}}}{\sqrt{A_{\mathrm{top0}}}} \tag{11}$$

However, only with appropriate constants (i.e., k_1, k_2, K_{CD}) was the relationship shown in Eq. (11) found to be suitable to fit the actual flight data; the constants should be specified for every balloon flight. In the present code, the varying drag coefficient with Eq. (11) could not be used because the proper

constants k_1, k_2, and K_{CD} for both HASI and ARD flight data are unknown. Another method to implement the varying drag coefficient in the simulation code is calculating the drag coefficient of the balloon during its ascent with the use of computational fluid dynamics (CFD). When calculating the drag coefficient using CFD, however, one should determine the shape of the envelope during the balloon's ascent, which takes some time, and generate mesh of the shape, which takes far more time. It needs many computational resources, so this work will be made in future research after securing plenty of computational resources. Instead, the present code keeps the drag coefficient of the balloon constant at a value of 0.45. The simulated results with the constant drag coefficient show a similar profile as the SINBAD and ACHAB programs when the constant drag coefficient of 0.45 is used for both programs.

On the left side of Fig. 3, the altitude profile of the present code seems to be similar to that of ACHAB with the constant drag coefficient. The codes with the constant drag coefficient predict a slightly faster rate of climb after approximately 2500 s, when the altitude of the balloon exceeds 10 km and the balloon enters the stratosphere. The reason is that the actual drag coefficient of the balloon increases as it passes through the stratosphere, where the ambient pressure drops and the balloon expands drastically. On the right side of Fig. 3, the result of the present code seems to follow a trajectory similar to that of SINBAD. Although the final altitude in the present code is predicted to be slightly higher than the other codes, the time when the balloon reaches its maximum altitude is approximately the same for the present code and SINBAD, as shown in the profile of the rate of climb. In summary, the present trajectory prediction program seems to yield reliably accurate results that are similar to

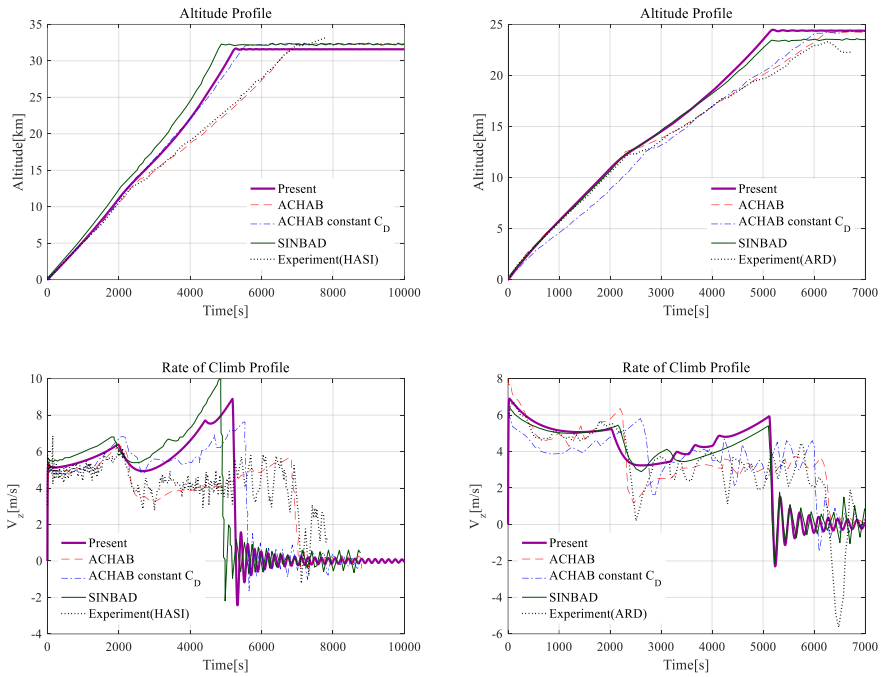

Fig. 3 Comparison of simulation results (Left: HASI, Right: ARD).

those of earlier programs. The program will be improved in future work so it can achieve higher prediction accuracy, with the varying drag coefficient implemented in ACHAB code, when compared with actual flight data.

E. Balloon Specifications and Flight Simulation Information

The balloon's specifications and the flight simulation information are presented in Table 1. The mass suspended by the envelope is assumed to be 10 kg, and the weight of the injected helium gas is 110% of the total weight of the balloon system except the buoyant gas. Because of the balloon design process introduced in Sec. II.A, the mass of the helium gas is 3.74 kg and the mass of the envelope is 11.34 kg because the thickness of the polyethylene film is assumed to be 20 μm and its density is assumed to be 940 kg/m^3. The total mass of the balloon system is 25.08 kg, and the fully inflated volume of the envelope is 1356.3 m^3.

The mission of the balloon flight is to ascend to an altitude of 30 km, collect atmospheric data, film its flight, and terminate the flight 5 h after launch. In the actual balloon operation, flight termination time can be chosen during the flight so that the flight mission is completed and the payload is retrieved in designated location. The simulation, however, focuses on the investigation on how the balloon moves, so it assumes the fixed duration of flight. The simulation assumes that the balloon is launched at Goheung, in the southern end of the Korean Peninsula. In the flight mission, due to the short endurance of the flight, dropping the ballast and opening the exhaust valve to control the rate of climb are not considered. The thermo-optical properties of the balloon film in [15] are used to calculate the forces on the balloon, and the simulation assumes the ground air temperature to be 288.15 K and the ground air pressure to be 101,325 Pa, which are the values given by the 1976 U.S. Standard Atmosphere.

Table 1 Balloon specification and flight simulation information

Parameter	Value
Balloon specification	
Suspending mass (parachute and payload)	10 kg
Free lift percentage	10%
Lifting gas mass	3.74 kg
Balloon mass	11.34 kg
Total mass	25.08 kg
Maximum volume	1356.3 m^3
Flight simulation information	
Target altitude	30 km
Flight termination	5 h after launch
Launch base	Goheung (lat: 34.623593, long: 127.185920)
Launch time	30 June 20150600 hrs local time (UTC +9)
Ground air temperature	288.15 K
Ground air pressure	101,325 Pa

To determine the launch date of the simulation, flight simulations for the mission were made using atmospheric data for the summer and winter of 2015 for approximately 30 days each. In the simulations, the launch times were set to 00:00, 0600, 1200, and 1800 hrs for each date to investigate how the

trajectory changes when the launch time varied. The weather data used in the simulations were provided by the Global Forecast System (GFS) model of the National Centers for Environmental Prediction, and the simulation used the GFS analysis file. Each numerical datum had a 0.5 deg grid resolution in both latitude and longitude, with a 26-layer vertical resolution.

Temperature, altitude, and wind velocity in the u and v directions are extracted from the weather data for each grid and vertical layer.

The simulation showed distinctive trends in the summer and winter. After the balloons flew eastward in the early hours, the direction of the wind changed westward at high altitudes in summer, whereas the wind blew only eastward in winter, as shown in Fig. 4. Because the balloon trajectory differed sensitively, depending on the date and time of launch, it was necessary when actually launching the scientific balloon to simulate the flight for several dates, varying the launch time and deciding a proper date. When deciding a proper launch date, the balloon should be predicted to barely move in the latitudinal direction during the flight for the balloon operation in the Republic of Korea. If the balloon was predicted to fly north, the balloon operators would terminate the balloon flight because most parts of the Republic of Korea are residential and the balloon landing would not be permitted due to the issue of safety. If the balloon was predicted to fly south, the balloon could intrude into Japanese territory, so the balloon operation would not be permitted. Therefore, in the simulation, the balloon was assumed to fly in summer days because of the tendency that the balloon would move eastward and come back westward at the higher altitudes. Finally, the balloon was assumed to be launched on June 30 at 0600 hrs local time [Coordinated Universal Time (UTC)/Greenwich Mean

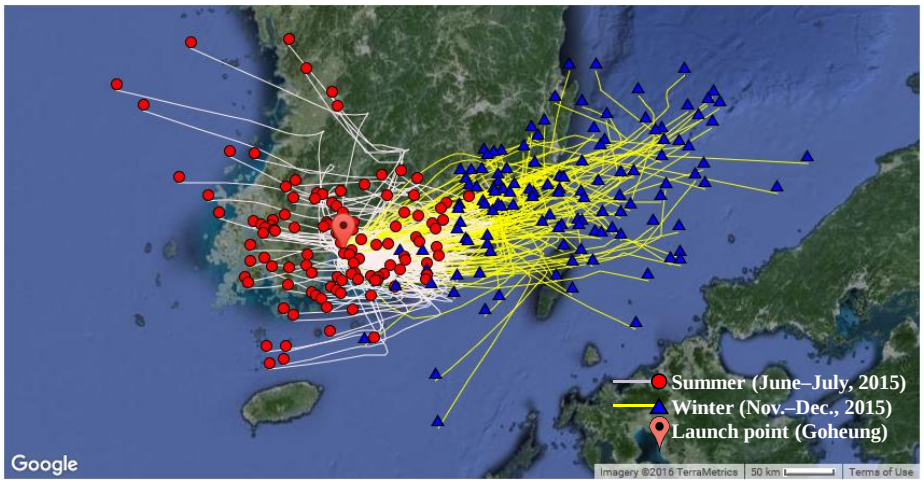

Fig. 4 Flight simulation during the summer and winter.

Time + 9 h] when the balloon was thought to be retrievable with minimum effort. At this launching time, the latitude component of the velocity profile was far smaller than the longitude component. In realistic balloon operation, the longitude of landing point could be controlled by adjusting the ascending speed by dropping ballasts and exhausting lift gas, as well as by choosing the time of flight termination, although the simulation assumed no use of ballast, no use of exhaust valve, and a fixed flight duration.

Figure 5 shows the deterministic trajectory of the target scientific balloon in latitude and longitude. The arrowed line, which represents the direction of flight, shows the trend of the balloon's movement after it is launched, which is summarized in the following steps:

1) The balloon initially moves northwestward.

2) The balloon moves eastward for a time.

3) The balloon flies southeastward.

4) The balloon flies westward until the flight is terminated.

From these four steps, one can picture the wind velocity profile throughout the flight. In steps 1 and 3, the latitudeward wind velocity component has opposite directions, and the component is negligible in steps 2 and 4, in which the longitudeward wind velocity component has opposite directions. Figures 6 and 7, respectively, show the simulated flight trajectory three-dimensionally (in latitude, longitude, and altitude), as well as the profiles of the altitude and the rate of climb with respect to flight time. The balloon reaches its maximum altitude 8800 s after the launch and keeps its altitude until the termination of the flight. Figure 8 shows the balloon envelope shape according to the altitude of the balloon during the flight. The shape rarely changes until the balloon reaches an altitude of approximately 5 km because the density of the ambient atmosphere decreases drastically when the balloon enters the stratosphere.

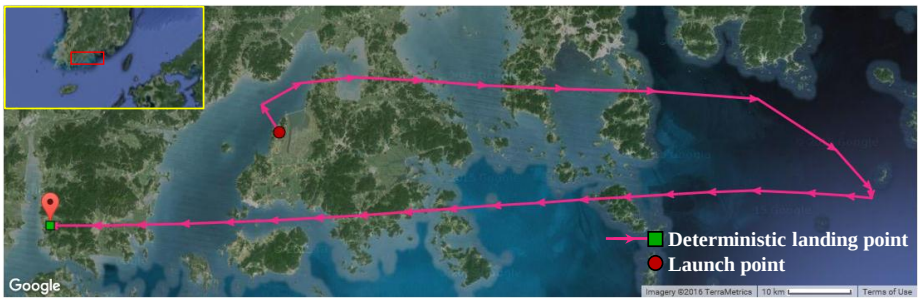

Fig. 5 Deterministic flight trajectory prediction of the target scientific balloon in latitude and longitude.

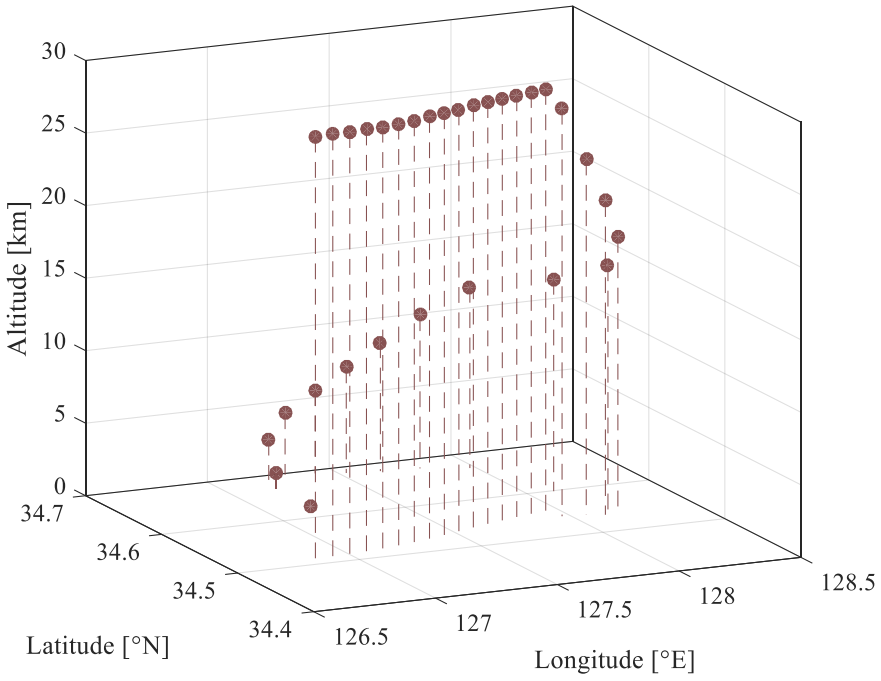

Fig. 6 Deterministic flight trajectory prediction of the target scientific balloon in latitude, longitude, and altitude.

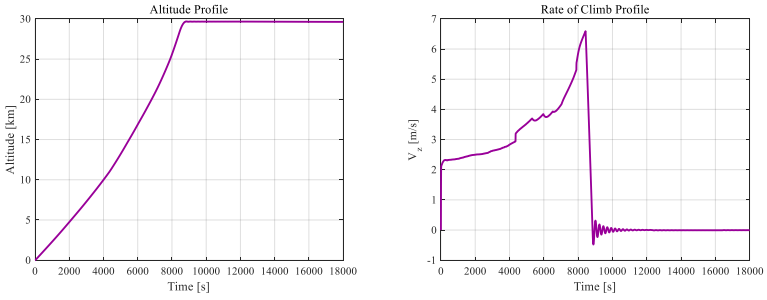

Fig. 7 Altitude and rate-of-climb profiles for the deterministic flight trajectory of the target scientific balloon.

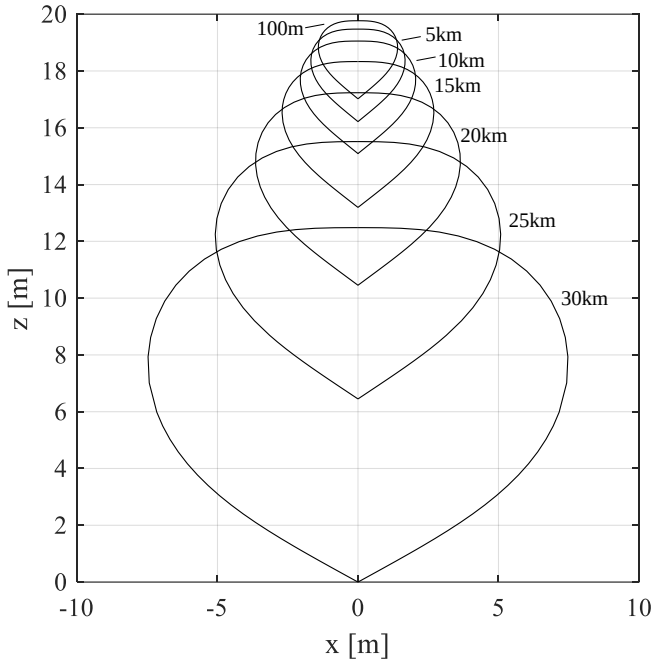

Fig. 8 Designed balloon shape for the simulation and its variance according to the altitude.

III. Uncertainty Analysis Based on Monte Carlo Simulation

Despite a careful modeling of the motion of a scientific balloon, there are some uncertainties that can degrade the accuracy of trajectory predictions. These uncertainties can be classified into four categories: operational uncertainty, uncertainty in the prediction model, environmental uncertainty, and manufactural uncertainty. Operational uncertainties occur when preparing the balloon for launch. For example, the amount of helium in the injecting process before launch involves uncertainty because there exists an error when measuring the mass of helium with the use of pressure gauges. Uncertainty in the prediction model includes the uncertainties in the dynamic model and the thermal model that the simulation program is using. In the dynamic model, the uncertainty occurs in the drag coefficient of the balloon, as calculating the drag coefficient of an ascending balloon in advance is not straightforward because the shape of the balloon keeps changing as it ascends and the balloon's shape may vary, depending on the weight of its payload. In the thermal model, the values of the terms used in the heat transfer equations change according to the atmospheric environment, but the prediction model uses an assumed value. As a result, the real thermal behavior is not appropriately implemented, so there exists an error in the predicted trajectory. Additionally, the simulation code does not describe the effusion of buoyant gas and icing problems, which are the other uncertainties in the prediction model. Environmental uncertainties are inevitable because the simulation uses predicted weather data and not the actual wind data, which include the wind velocity profile, the ambient temperature,

and the ambient pressure. Manufactural uncertainty may occur when the gores of the envelope are manufactured and sealed, which affects the volume of the envelope. Moreover, after load tapes are attached and the exhaust valve and venting ducts are equipped, the shape of the balloon differs from the natural balloon shape that the simulation code assumes.

In addition to the aforementioned examples of uncertainties, many other uncertainties can occur during the actual flight that the simulation program cannot predict. Because considering all of the uncertainties is unrealistic, the present paper focuses on selected uncertainties. Based on earlier studies [10,11], the amount of helium gas injected in the envelope before launch is selected to represent the operational uncertainty. Although the amount of the lifting gas can be controlled during the actual flight for a zero-pressure balloon, a sensitivity study on the amount of gas is still meaningful because it allows one to understand how the operational uncertainty affects the trajectory of a balloon and to prepare for a malfunction of the buoyancy control unit in the balloon system, such as the exhaust valve or ballasting equipment. Additionally, the drag coefficient of the balloon is chosen for the uncertainty in the prediction model, and the forecasted wind profile to be used in the simulation is selected for the environmental uncertainty. In the case of the drag coefficient, understanding the effect of its uncertainty is important because the present simulation code uses a constant drag coefficient, whereas it varies in the realistic balloon operation. If the effect is found to be significant, varying the drag coefficient will have to be implemented in the simulation code. For the manufactural uncertainty, the maximum volume of the balloon, which is thought to affect the trajectory but was not considered in earlier works, is

additionally taken into account in the present work. The Monte Carlo simulation is made for the analysis of each uncertainty, where the sample points are selected by generating uniformly distributed random numbers between zero and one for each random variable and obtaining corresponding values from each random variable distribution.

A. Operational Uncertainty: Uncertainty in Helium Injection

Buoyant gas injected into a scientific balloon before launch is measured with a pressure gauge. Unfortunately, during this process, the exact amount of gas is unknown due to the inherent error in the pressure gauge. Additionally, the result of calculation using some equations might be different from the exact value of the mass of the gas because the equations usually have assumptions to make the calculation easier. As mentioned earlier, the amount of the lifting gas can be controlled in the actual flight with the use of the exhaust valve (if there is an excess in the amount of gas) and ballasting if the buoyancy is insufficient. The uncertainty study, however, is still meaningful, as it can help one plan the balloon mission. The uncertainty in helium injection could be neglected if its influence on the balloon trajectory is negligible or if the spare lifting gas and ballast are sufficiently prepared to control the buoyancy and preserve the mission flight time if the uncertainty in helium injection yields significant error. According to earlier experience, the error in the mass of the buoyant gas is known to fall within the range of 1 to 2% during injection [16]. To determine the influence of the uncertainty in the mass of buoyant gas on the trajectory of the balloon, 10,000 trajectories are simulated with the Monte Carlo analysis. In the present work, the error is thought to be normally distributed, as it is a common assumption for unknown distributions. The standard deviation and the mean value of the distribution of free lift ratio are set to 0.02 and 1.1, respectively. The value of the free lift ratio is multiplied by the weight of the balloon system to calculate the amount of helium gas.

B. Uncertainty in the Prediction Model: Uncertainty in the Drag Coefficient

The present simulation code uses the value of 0.45 for the constant drag coefficient of the scientific balloon throughout the whole flight, as earlier programs did. Although the simulation uses a constant drag coefficient, the actual flying scientific balloon has varying drag coefficients because the volume and shape of the envelope change. Additionally, the value of 0.45 is inadequate for the drag coefficients of all scientific balloons because they have various shapes according to their missions. In the present simulation code, the drag coefficient of the balloon is used to calculate the drag forces in the *x*, *y*, and *z* directions so that the balloon's rate of climb and its velocity in the latitudinal and longitudinal directions are obtained, which is essential to predict the trajectory of the balloon. Thus, the simulated trajectory with the constant drag coefficient is likely to be different from the actual trajectory, and it should be clarified how the uncertainty in drag coefficient affects the trajectory. If the error arising from the uncertainty in the drag coefficient is insignificant, the assumption of a constant drag coefficient will be sufficient for the prediction of the balloon trajectory. Otherwise, a thorough study of the drag coefficient of the balloon will have to be made. Assuming that the earlier works used the value of 0.45 for the drag coefficient for some reason, the Monte Carlo simulation is made for a normal distribution of the drag coefficients with a mean value of 0.45 and 10,000 predicted trajectories. The value of the standard deviation of the distribution is assumed to be 0.1, which is approximately 20% of the mean value. This is found to be a moderate assumption because the effect

of the uncertainty could be remarkable.

C. Environmental Uncertainty: Uncertainty in the Wind Profile Data

The trajectory of a balloon is greatly affected by the wind profile because the horizontal movement of the balloon is caused only by the drag force acting on it. In fact, the velocity of the balloon can be assumed to be identical to the wind velocity during the entire flight, as the balloon is accelerated to the wind velocity in a short time. Accordingly, the uncertainty in the wind profile data will directly affect the prediction of the trajectory of a balloon. The present simulation code uses numerical weather data provided by the GFS model to obtain the wind velocity profile. Because the weather data are calculated results from a weather model, and not the actual measured data, there should be an uncertainty in the wind profile that yields the difference between the actual and simulated trajectories of the balloon. If the environmental uncertainty affects the flight trajectory of a scientific balloon more than any other uncertainties, the procedure to determine when to launch a balloon will have to be carefully established.

To identify the effects of the uncertainty in the wind profile on the trajectory of a balloon, a Monte Carlo simulation was performed, and 10,000 trajectories were predicted by disturbing the wind velocity profile in the simulation. To disturb the wind profile, the wind velocity data were uniformly distributed in both longitude and latitude. This was because the uncertainty in the wind profile was thought to have more severe randomness than any other uncertainty. It was difficult to predict the fluctuation in the actual wind velocity profile because adjacent altitudes in the troposphere had a severe correlation. Also, the

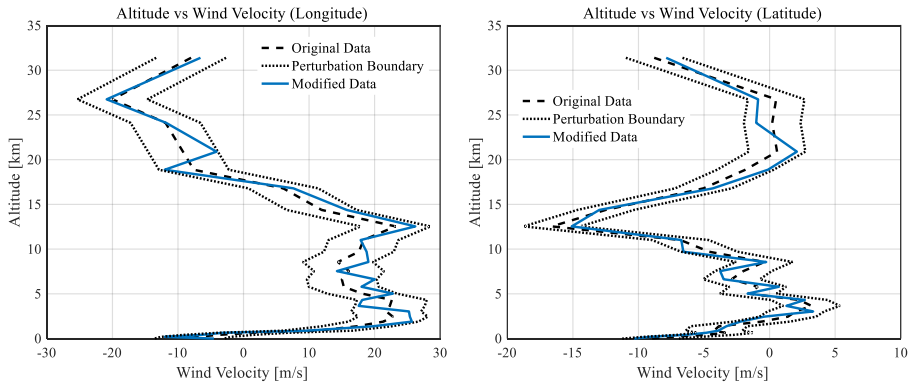

Fig. 9 Example of the disturbed wind profile with the use of uniform distribution.

fluctuation could become larger at the altitudes between 10 and 15 km, where the wind speed tended to be fast. Uniform distribution was thought to reflect the irregularity of wind fluctuation, and thus to distribute the wind velocities as randomly as possible. Within the weather data grid, the data in the area of 33–37° for latitude and 122–132° for longitude were modified for 26 vertical layers. Because the grid had a 0.5 deg resolution, two 9-by-21 matrices that consisted of uniformly distributed numbers between −0.1 and 0.1 were multiplied by the maximum values of the longitudinal and latitudinal velocities, respectively, for each vertical layer. They were then added to the matrices of the wind data so that the wind profile was perturbed within the error boundary of 10% of the maximum velocity. Given that the accuracy of the weather model GFS was unknown, the error boundary of 10% of the maximum velocity in the data was thought to be a moderate assumption because the model would not have any usefulness if it had an error of more than 10% of the maximum value in the calculated results. An example of the disturbed wind profile by uniform

distribution is shown in Fig. 9. The assumption of uniform distribution might still have limitation, but the disturbed wind profile shown in Fig. 9 seems to qualitatively agree with the actual complex wind profile.

D. Manufactural Uncertainty: Uncertainty in the Volume of the Balloon

In the manufacturing process, the total volume of the balloon can become different from the designed volume because the engineering tolerance should be taken into account. The volume of the envelope is used to calculate the drag force and the buoyant force, so the uncertainty in the volume is thought to have a strong influence on the trajectory. The error in the volume of the balloon depends on the manufacturing reliability, so a study of how to make the envelope manufacturing process reliable should be before any other works of scientific ballooning if the manufactural uncertainty dominates the error in trajectory prediction. In the present work, the manufacturing error is assumed to be normally distributed with its mean value as one and a standard deviation value as 0.01. The assumption on the standard deviation value seems to be reasonable because a manufacturing error of more than 1% of the designed balloon will make the design process worthless. The effects derived from the differences in the volume of designed and manufactured balloons are examined using a Monte Carlo simulation. In the simulation, 10,000 trajectories are predicted, with the designed volume being multiplied by a random value of the manufacturing error distribution.

E. Results and Discussions

Figures 10–14 show the simulation results of varying each uncertainty parameter mentioned earlier. The distributions of the 10,000 landing points are represented in the form of a heat map in latitude–longitude axes, with the use of Google Maps. To make the heat maps, the diameter of the circle that shows the influence area of each data point is set to 2.5 km, and the maximum intensity is varied between 50 and 3000 with respect to each result. Simulated data varying each uncertainty parameter are filtered before making the heat map, so that every point in the filtered dataset is included within three sigma of the mean values of both the latitude and longitude distributions of the landing points.

Figure 10 shows the simulation results considering all uncertainties the present work considers: operational uncertainty, uncertainty in the prediction model, environmental uncertainty, and manufactural uncertainty. The area of the heat map of the landing points is broad, with a latitude range of approximately 20 km and a longitude range of approximately 120 km. This result shows that the deterministic prediction of the flight trajectory is meaningless. The uncertainty that causes the broad landing point distribution should be noteworthy, and its influence should be minimized for the flight trajectory prediction to become meaningful.

Figure 11 shows the results of the Monte Carlo simulation varying the amount of helium gas injected. Because the free lift ratio was normally distributed, the landing points seemed to have normal distributions for both the longitude and latitude directions, which concentrated the landing points near the deterministic landing point and resulted in the linear shape of the heat map. The heat map

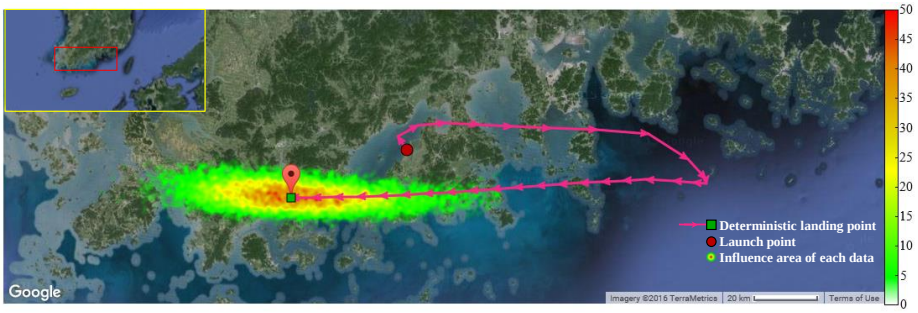

Fig. 10 Landing point distribution considering all uncertainties.

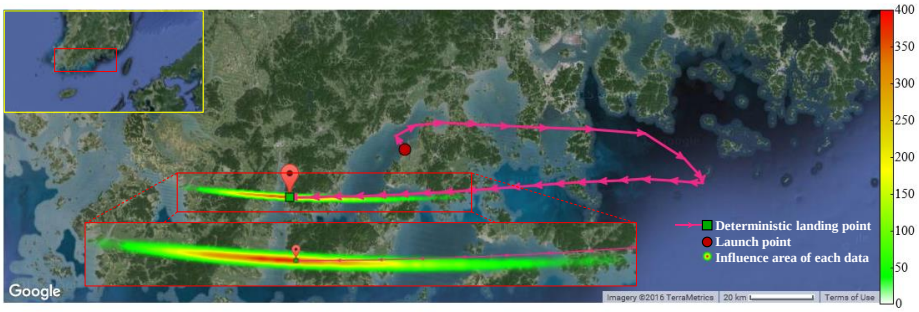

Fig. 11 Landing point distribution considering the uncertainty in helium injection.

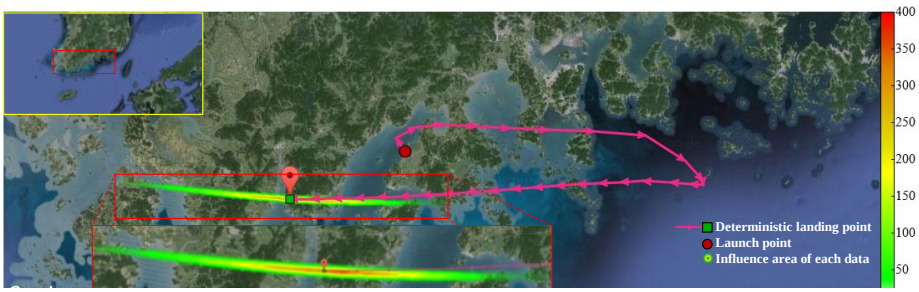

Fig. 12 Landing point distribution considering the uncertainty in drag coefficient.

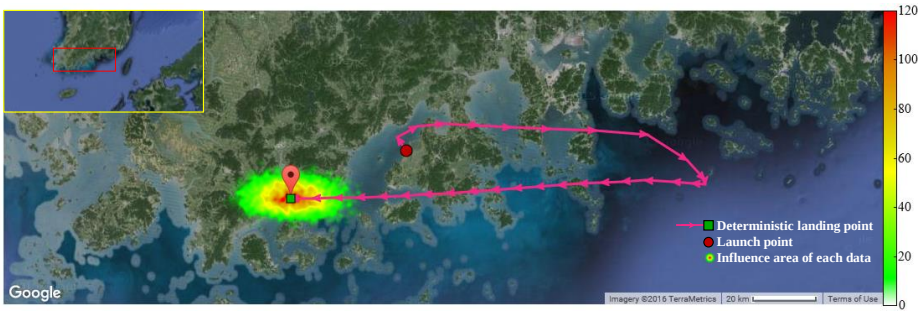

Fig. 13 Landing point distribution considering the uncertainty in the wind profile data.

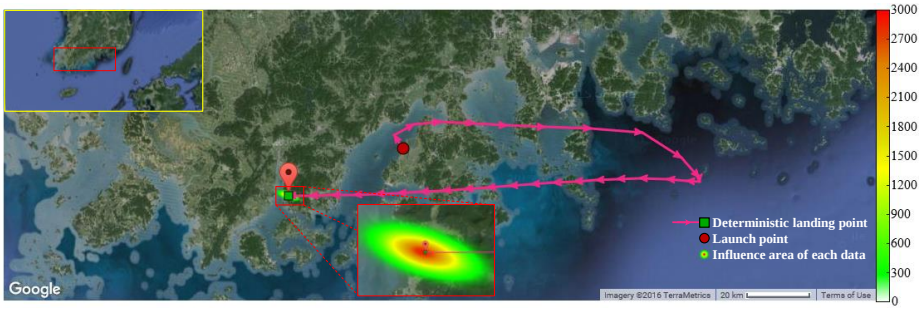

Fig. 14 Landing point distribution considering the uncertainty in the volume of the manufactured envelope.

was mostly spread in the longitude direction because the latitude distribution of the landing points had a small standard deviation value. The difference between the maximum and minimum latitudes of the landing points was 0.0400°, whereas the difference between the maximum and minimum longitudes was 1.0061°, which was approximately 25 times greater. One reason the landing points were not affected latitudewise by the uncertainty in the free lift ratio was that the latitudewise component of the wind velocity during the whole flight was much smaller than the longitudewise component. As mentioned earlier, the

flight of the scientific balloon in the simulation consisted of four steps. By comparing the distance of the balloon's movement in steps 1 and 3 and in steps 2 and 4, as introduced in Sec. II.E, it could be seen that the distance in steps 2 and 4 was much greater. If the same error percentage was multiplied, the resultant distance error was likely to be larger when the multiplied distance was greater. From this point of view, a greater distance meant a faster wind velocity because the distance was proportional to wind velocity and the time the balloon faced the wind, so the wind velocity profile would be one reason for the linear shape of the heat map. It should be noted that the present balloon launching time of the simulation brought this particular result. In some realistic balloon operation environment and in another balloon launching time, the result could be shown to be completely different so that the landing points were not affected longitudewise by the uncertainty in the free lift ratio.

The difference in latitude and longitude distributions of the landing points can also be explained with Fig. 15. On the left of Fig. 15, which describes the movement of the balloon in the altitude–latitude axes, one can observe that the latitudinal movement occurs when the balloon is at an altitude of approximately 0–5 km, at 10–15 km, and at its target altitude of 30 km. Because the distance the balloon moves at the target altitude is less than the distances at the altitudes of 0–5 and 10–15 km, the latitude of the landing points depends greatly on the movement of the balloon at the altitudes of 0–5 and 10–15 km. In those ranges of altitudes, however, the direction of the movement is opposite, and it can be observed that the distances in those altitudes are both long and short so that the sum of the distances rarely changes when comparing the trajectory profiles of points A and B.

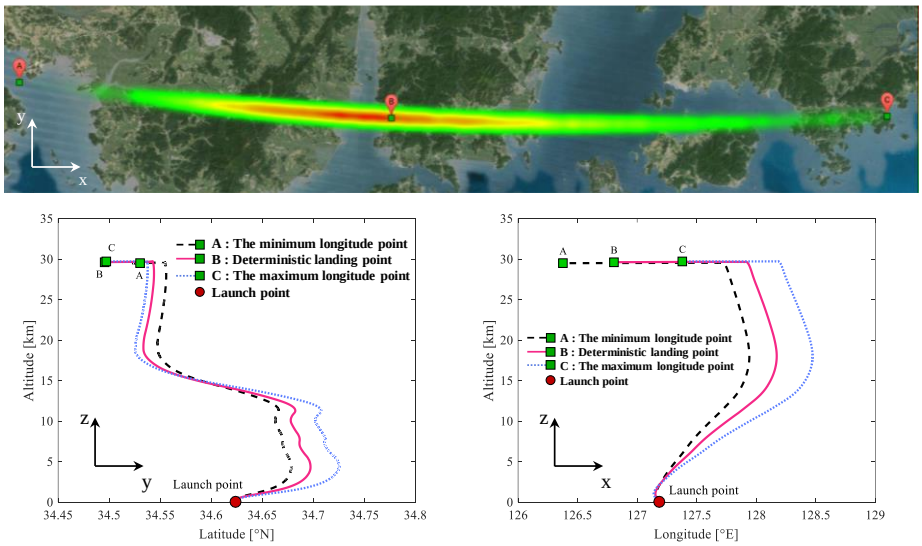

Fig. 15 Monte Carlo simulation results varying the helium gas percentage (left : altitude-latitude axes / right: altitude-longitude axes).

On the other hand, the longitudinal movement of the balloon occurs throughout the flight, and the direction of the movement changes when the balloon arrives at the altitude of 15 km, as shown on the right side of Fig. 15, which describes the movement of the balloon in the altitude–longitude axes. Unlike the latitudinal direction, the time when the balloon reaches the altitude of 15 km decides the longitude of the landing point because the flight termination time is determined to be 5 h after the launch of the balloon. Because the free lift ratio decides the rate of climb of the scientific balloon, it is reasonable that the longitudinal distribution of the landing points is sensitive to the uncertainty in the free lift ratio. On the left and right sides of Fig. 15, one will realize that the rate of climb of the trajectory of point A is faster than the rate of climb of the trajectory of point C because the distance of the balloon's movement is greater in the case of point C within a certain altitude range. As

mentioned before, the distance of the balloon's movement is proportional to the wind velocity and the time it flies at a certain altitude range, and a longer distance means a longer time of flight because the wind velocity profile is given as constant at a certain altitude range. Actually, points A and C are also the points where the free lift ratio is given its maximum and minimum, respectively, so the rates of climb are the maximum and minimum, respectively. In this simulation, it turns out that the longitude of the landing point moves westward as the amount of buoyant gas injected into the envelope increases.

To find the relation between the free lift ratio and the longitude of the landing point, the rate-of-climb profiles with maximum, mean, and minimum values of the free lift ratio, which are normally distributed with a standard deviation value of 0.02, are depicted in Fig. 16. Because the free lift ratio of the balloon is directly and proportionally related to the buoyant force, and because the free lift ratio values have a linearly proportional relation, the initial velocities of the trajectories of points A, B, and C also show a linearly proportional relation. The times taken for a scientific balloon to reach a certain altitude are inversely proportional if the velocities have a linearly proportional relation. Thus, the free lift ratio and the time to reach a certain altitude have an inversely proportional relation. The longitudinal distance of the balloon is calculated by multiplying the longitudinal velocity of the balloon by the time the balloon flies at a certain altitude, which results in the asymmetry in the distribution of predicted landing points. To obtain a symmetric distribution of landing points, plenty of time to fly after the altitude of 15 km, where the longitudinal wind velocity changes its direction, should be given to the balloon to compensate for the distance crossed before reaching the altitude of 15 km. Because there exist some points at which

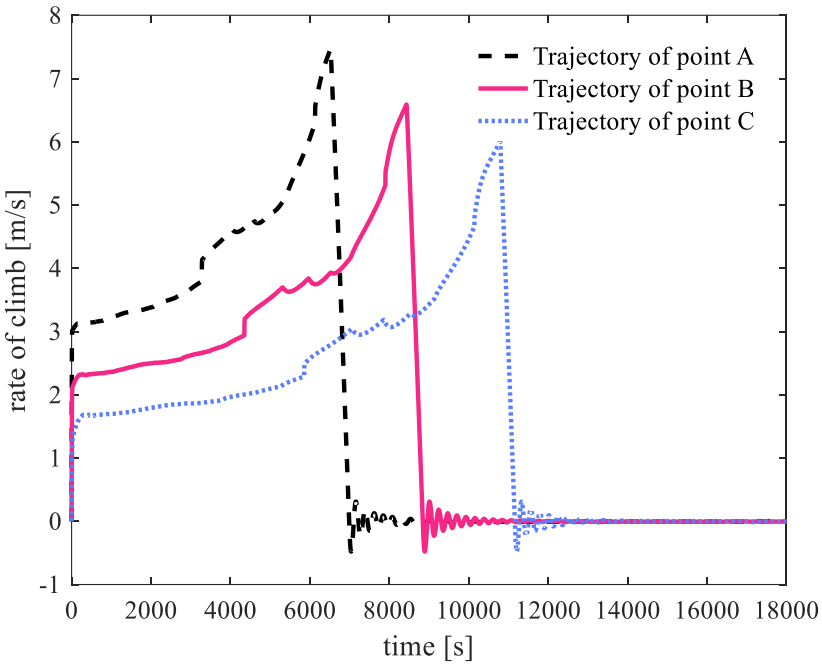

Fig. 16 Rate-of-climb profiles of the trajectories of points A, B, and C in Fig. 15.

the rate of climb is too slow to compensate for the rightward movement, the final distribution of landing points leans to the left for this simulation.

Figure 12 shows the results of the Monte Carlo simulation varying the drag coefficient of the balloon. Because the value of the standard deviation was larger in the longitudinal direction, the heat map in Fig. 12 has a linear shape like the heat map in Fig. 11. Because the same wind profile was used in the simulations considering the uncertainties in the free lift ratio and the drag coefficient of the balloon, the reason the difference occurs in the latitude and longitude distributions of the landing points would be the same as the reasons mentioned before. In this simulation with the standard deviation value of the

drag coefficient of 0.1, the difference between the maximum and the minimum latitudes of the landing points was 0.0574°, and the difference between the maximum and the minimum longitudes was 1.1379°, which was approximately 20 times greater. The ratio of differences was a little smaller than the ratio of differences when the free lift ratio was distributed with the standard deviation value of 0.02. This meant that the difference between the maximum and minimum longitudes of landing points would be greater when the free lift ratio was normally distributed, if the difference between the maximum and minimum latitudes was the same with some adjustment in the standard deviation values of the drag coefficient and the free lift ratio distributions. Thus, the trajectory of a scientific balloon was more sensitive to the uncertainty in the amount of helium gas.

In the left and right sides of Fig. 17, one can see that the trajectories of points A and C are symmetric to the trajectory of point B in both the altitude–latitude and altitude–longitude axes, given that A and C are where the landing points are the minimum and maximum, respectively. The drag coefficients of the balloon used in the simulations of points A and C are 0.1874 and 0.7958, which are the minimum and maximum values, respectively, of the drag coefficient distribution with a standard deviation value of 0.1. It turns out that, the greater the drag coefficient of the balloon, the higher the longitude of the predicted landing point in this simulation. Because the distribution of the landing points turns out to be normally distributed, like the distribution of the input drag coefficient, the longitude of the landing point and the drag coefficient of a scientific balloon have a linear proportional relation in this simulation.

Comparing the shapes of the heat maps in Figs. 11 and 12, one can see that

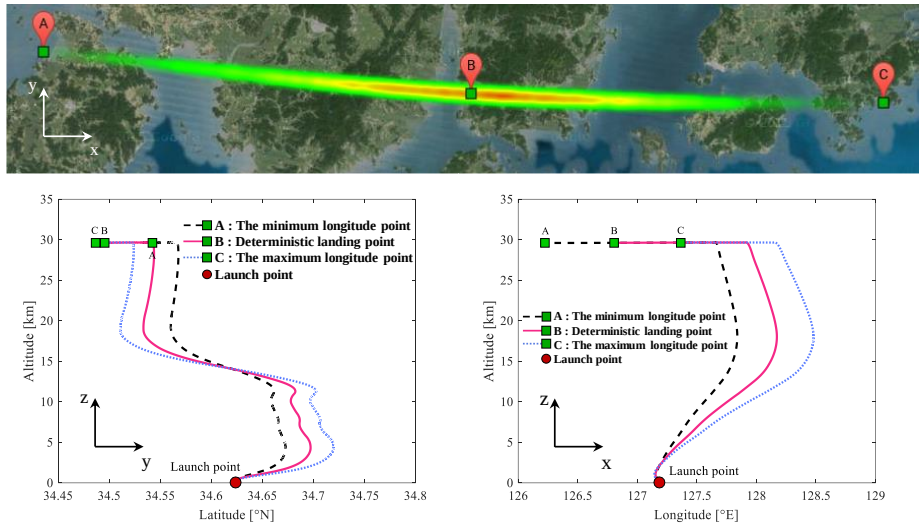

Fig. 17 Monte Carlo simulation results varying the drag coefficient (left : altitude-latitude axes / right: altitude-longitude axes).

the trend of the shape is different. When the uncertainty in the free lift ratio is considered, the heat map has a tail in the right direction, whereas the heat map in Fig. 12 has a nearly symmetric shape. In the simulation in which the free lift ratio is distributed, the behavior of the balloon can be explained in terms of the rate of climb because the free lift ratio affects it. Because the velocity of the scientific balloon is approximately the same at a given altitude, regardless of the drag coefficient of the balloon and because the drag coefficient only affects the rate of climb, the behavior of the balloon when its drag coefficient is varied would also be explained in terms of the rate of climb. The trajectories of points A, B, and C in Fig. 12 are redrawn in Fig. 18 in the rate-of-climb/time axes. One can see that the initial velocities of the points are inversely rather than linearly proportional, in contrast to the result in Fig. 16. Because the drag coefficient is used to calculate the drag force on the balloon, which interrupts

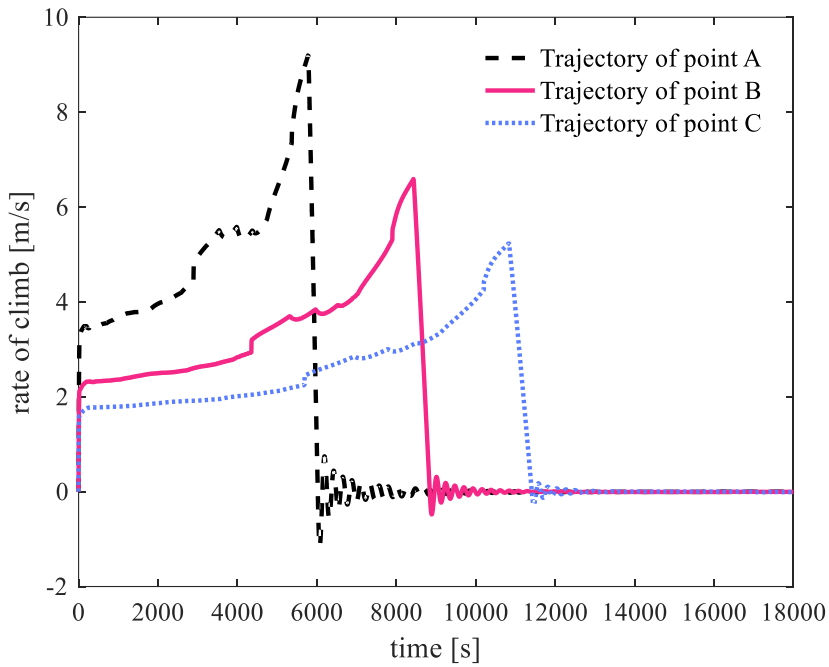

Fig. 18 Rate-of-climb profiles of the trajectories of points A, B, and C in Fig. 17.

the ascending motion of the balloon, the rate of climb inevitably has an inversely proportional relation with the drag coefficient of the balloon. Because the time to reach a given altitude for a balloon is inversely proportional to its velocity, the drag coefficient of the balloon and the time it flies at a certain altitude have a proportional relation. As mentioned before, the distance a balloon moves in a longitudinal direction is calculated by multiplying the time and the wind velocity at the present altitude. Because the time to reach a certain altitude and the drag coefficient have a linearly proportional relation, the ratio between the distance the balloon flies and the drag coefficient of the balloon is consistent along the altitude, which results in the symmetric and linear shape of

the heat map in Fig. 12.

Figure 13 shows the results of Monte Carlo simulation varying the wind profile. Unlike the distribution of landing points when considering the uncertainties in the amount of lifting gas and the drag coefficient of the scientific balloon, the heat map of landing points when the wind profile was varied made a circular shape in Fig. 13. The change in the latitudinal component of the wind profile caused this outcome; thus, this result shows how large an effect the wind profile has on the trajectory of a scientific balloon. Although the wind velocity profile was perturbed with an error boundary of 10% of the maximum value in the wind velocity dataset, the difference between the maximum and minimum longitudes was 0.3550°, which was a far smaller value than the values for landing points in Figs. 11 and 12. Because the changed wind profile greatly varied the latitudes of the landing points, the difference between the maximum and the minimum latitudes was found to be 0.1808°, which was much larger than any other values for landing points with other uncertainties. In terms of longitude, the sensitivity of the uncertainty in the wind profile on the trajectory of the balloon seemed to not be as much as the uncertainties in the amount of buoyant gas and the drag coefficient of the balloon. Although the wind velocity profile data were perturbed in uniform distribution, the simulated landing points were concentrated around the deterministic landing point, forming a normal distribution and following the central limit theorem. Because controlling the uncertainty in the wind profile in the actual balloon flight was nearly impossible, the error boundary of the landing points considering the uncertainty in wind profile data was determined to be within an acceptable error range in the present work; the distance between the maximum and minimum

longitudes of the boundary was approximately 40 km. To meet the acceptable error, the standard deviation of the distribution of the free lift ratio had to be 0.007 so that the error in injecting the lifting gas hardly exceeded 2%, following the three-sigma rule. The standard deviation of the normal distribution of the drag coefficient should be less than 0.032. The assumption that the constant drag coefficient of the balloon was 0.45 would be invalid if the actual value of the drag coefficient exceeded the limit of 0.354–0.546, which was attained by the three-sigma rule.

Figure 14 shows the results of the Monte Carlo simulation varying the volume of the balloon. It can be seen that the distribution range of the landing points is smaller than that of any other uncertainty. Because the velocity data are not changed, the zoomed-in figure shows that the heat map of the landing points forms a linear shape. Because the manufactural tolerance is thought to hardly exceed 1%, it seems that the influence of manufactural uncertainty on the balloon flight is negligible. Thus, in the perspective of the trajectory prediction, it would be tolerable for the balloon manufacturer to make a minor change in the shape of the envelope if there is confidence that the balloon can achieve its mission successfully.

IV. Conclusions

Predicting the flight trajectory of a scientific balloon is important to avoid accidents, as controlling the horizontal motion of a flying balloon is nearly impossible. Because deterministic prediction hardly matches the actual flight trajectory, the prediction should be made in a probabilistic manner, considering the uncertainties involved in the actual balloon flight. The uncertainties can be categorized into operational uncertainty, uncertainty in the prediction model, environmental uncertainty, and manufactural uncertainty.

In the present work, the trajectories of a scientific balloon were numerically predicted considering various uncertainties with the use of Monte Carlo simulation. For the simulation, a program for predicting balloon trajectories was developed and validated against earlier numerical programs. The uncertainties considered in the present work included all of the categories of the uncertainties. The amount of helium gas injected before launching the balloon was considered as the operational uncertainty, and the drag coefficient was selected to represent the uncertainty in the prediction model. Wind profile data represented the environmental uncertainty, and the volume of the envelope was chosen as the manufactural uncertainty. The distributions of the free lift ratio, the drag coefficient, and the error percentage of the manufactured volume of the envelope were thought to be normal distributions, and the distribution of the error in the wind velocity profile was assumed to be a uniform distribution.

1) Integrating all four uncertainties, the results of 10,000 Monte Carlo simulations made a broad elliptical area of possible landing points, which had longitudinal diameters of approximately 120 km. To capture the dominant

uncertainty parameter that yielded this broad error boundary, an additional 10,000 Monte Carlo simulations were performed, varying each uncertainty parameter while keeping the other parameters constant.

2) Among the uncertainties, the amount of helium gas, representing the operational uncertainty, was shown to have the most substantial effect on the trajectory. Nonetheless, the amount of helium gas could be controlled during the actual flight, so control of the amount of lifting gas would be reliably prepared to make the actual flight trajectory fit the predicted flight trajectory if one needed to minimize the difference between the two. Uncertainty in the drag coefficient was the next dominant uncertainty parameter. Therefore, using a constant drag coefficient to predict the trajectory of a balloon flight was incomplete, and thorough studies on calculating the varying drag coefficient have to be made in future works. Uncertainty in the wind profile along the altitude, which represented environmental uncertainty, was shown to have less effect on the balloon trajectory, even though it was the main source of the horizontal motion of the balloon.

3) Given that the prediction error derived from the wind profile data cannot be controlled, its error boundary was determined to be the target error range of the trajectory simulation. To meet the error boundary, the standard deviation values of the distribution of the free lift ratio had to be 0.007 and 0.032 in the case of the drag coefficient distribution. Finally, uncertainty in the volume of the manufactured envelope showed little effect on the trajectory of the balloon. Thus, one could neglect a slight change in the shape of the manufactured envelope from the conceptual design, as it would not cause failure of the mission of the balloon flight unless the balloon burst during the flight.

Appendix A: Specific Procedures to Design a Natural Shape Balloon

As shown in Fig. A1, the shape of a balloon envelope can be made by rotating curve C with respect to the A axis. The length from the base along curve C is denoted by *s*, and the distance from the curve to the A axis is represented by *r*. The altitude of the balloon apex and the base are referred to as *z* and z_b, respectively. The meridional angle between the line tangent to curve C and the A axis is denoted by θ, and the angle in a plane perpendicular to the A axis is represented by φ. The actual mass per unit area of balloon film is referred to as we, and the pressure difference between the inside and the outside of the balloon film is Δp. The tension per unit length when φ is constant is denoted by T_θ, and T_φ refers to the tension per unit length when θ is constant. The procedure to design the balloon shape starts with the following equations of force equilibrium on the surface of the envelope:

$$\begin{aligned}&\left(T_\theta+\frac{\mathrm{d}T_\theta}{2}\right)\left(r+\frac{\mathrm{d}r}{2}\right)\mathrm{d}\varphi\cos\left(\theta+\frac{\mathrm{d}\theta}{2}\right)\\&-\left(T_\theta-\frac{\mathrm{d}T_\theta}{2}\right)\left(r-\frac{\mathrm{d}r}{2}\right)\mathrm{d}\varphi\cos\left(\theta-\frac{\mathrm{d}\theta}{2}\right)\\&-r\mathrm{d}\varphi w_e g\mathrm{d}s-r\mathrm{d}\varphi\Delta p\mathrm{d}s\sin\theta=0\end{aligned}\tag{A1}$$

$$\begin{aligned}&\left(T_\theta+\frac{\mathrm{d}T_\theta}{2}\right)\left(r+\frac{\mathrm{d}r}{2}\right)\mathrm{d}\varphi\sin\left(\theta+\frac{\mathrm{d}\theta}{2}\right)\\&-\left(T_\theta-\frac{\mathrm{d}T_\theta}{2}\right)\left(r-\frac{\mathrm{d}r}{2}\right)\mathrm{d}\varphi\sin\left(\theta-\frac{\mathrm{d}\theta}{2}\right)\\&-2T_\varphi\mathrm{d}s\sin\frac{\mathrm{d}\varphi}{2}+r\mathrm{d}\varphi\Delta p\mathrm{d}s\cos\theta=0\end{aligned}\tag{A2}$$

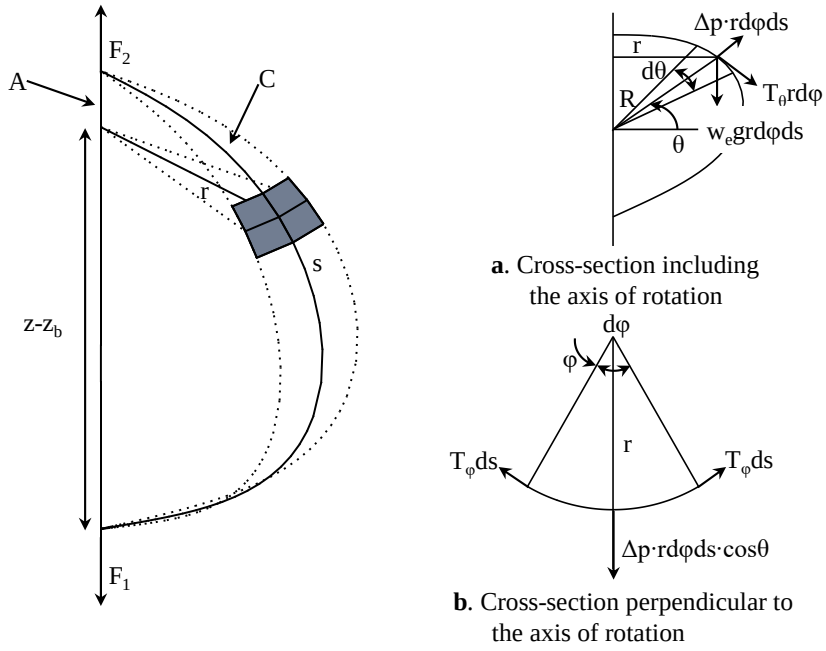

Fig. A1 Balloon surface elements: a) Cross-section including the axis of rotation, and b) Cross-section perpendicular to the axis of rotation

Equation (A1) depicts the force equilibrium in the *z* direction, and Eq. (A2) depicts that for the *r* direction. Each term used in the equations is described in Figs. A1a and A1b. Eliminating the higher order terms in Eqs. (A1) and (A2), the following equations are obtained:

$$\begin{aligned} &\frac{\mathrm{d}(rT_\theta)}{\mathrm{d}s}\cos\theta - rT_\theta \sin\theta \frac{\mathrm{d}\theta}{\mathrm{d}s} - rw_e g - \Delta pr\sin\theta = 0, \\ &\frac{\mathrm{d}(rT_\theta)}{\mathrm{d}s}\sin\theta + rT_\theta \cos\theta \frac{\mathrm{d}\theta}{\mathrm{d}s} - T_\varphi + \Delta pr\cos\theta = 0 \end{aligned} \tag{A3}$$

Rewriting Eq. (A3) gives the following:

$$
\begin{aligned}
rT_\theta \frac{\mathrm{d}\theta}{\mathrm{d}s} &= T_\varphi \cos\theta - rw_e g \sin\theta - \Delta p r, \\
\frac{\mathrm{d}(rT_\theta)}{\mathrm{d}s} &= T_\varphi \sin\theta + rw_e g \cos\theta
\end{aligned}
\tag{A4}
$$

It is assumed that there are no load tapes on the target balloon, so the tension on the surface of envelope in the meridional direction T_φ becomes zero. With the equations $\Delta p = (\rho_a - \rho_g) g (z - z_b)$ and $b_g = (\rho_a - \rho_g) g$, which represent the effective buoyant force per unit volume, Eq. (A4) can be rewritten as follows:

$$
\begin{aligned}
rT_\theta \frac{\mathrm{d}\theta}{\mathrm{d}s} &= -rw_e g \sin\theta - b_g (z - z_b) r \\
\frac{\mathrm{d}(rT_\theta)}{\mathrm{d}s} &= rw_e g \cos\theta
\end{aligned}
\tag{A5}
$$

From the geometrical considerations in Fig. A1, the following equations can be found:

$$
\frac{\mathrm{d}r}{\mathrm{d}s} = \sin\theta, \quad \frac{\mathrm{d}z}{\mathrm{d}s} = \cos\theta, \quad \frac{\mathrm{d}S}{\mathrm{d}s} = 2\pi r, \quad \frac{\mathrm{d}V}{\mathrm{d}s} = \pi r^2 \cos\theta \tag{A6}
$$

Defining the dimensionless length λ, which represents the ratio between the external forces acting on the film of the balloon and the effective buoyant force per unit volume, the dimensionless parameters can be defined as follows:

$$
\begin{aligned}
&\tilde{r} = \frac{r}{\lambda}, \quad \tilde{z} = \frac{z}{\lambda}, \quad \tilde{z}_b = \frac{z_b}{\lambda}, \quad \tilde{s} = \frac{s}{\lambda}, \quad \tilde{l}_s = \frac{l_s}{\lambda}, \quad \tilde{R} = \frac{R}{\lambda}, \\
&\tilde{S} = \frac{S}{\lambda^2}, \quad \tilde{V} = \frac{V}{\lambda^3}, \quad \lambda = \left(\frac{F_1 + F_2}{b_g} \right)^{1/3}
\end{aligned}
\tag{A7}
$$

where F_1 and F_2 are the external forces acting on the apex and the base of the balloon film, respectively.

Because the balloon under consideration is assumed to have a payload system

suspended from a single envelope, F_1 has a zero value and F_2 is equal to the weight of the suspending payload system. Using the parameters in Eqs. (A7), Eqs. (A5) and (A6) become

$$\tilde{r}\tilde{T}_\theta \frac{\mathrm{d}\theta}{\mathrm{d}\tilde{s}} = -k\Sigma_e \tilde{r} \frac{\mathrm{d}\tilde{r}}{\mathrm{d}\tilde{s}} - (\tilde{z} - \tilde{z}_b)\tilde{r}$$

$$\frac{\mathrm{d}(\tilde{r}\tilde{T}_\theta)}{\mathrm{d}\tilde{s}} = k\Sigma_e \tilde{r} \frac{\mathrm{d}\tilde{z}}{\mathrm{d}\tilde{s}}$$

$$\frac{\mathrm{d}\tilde{r}}{\mathrm{d}\tilde{s}} = \sin\theta, \quad \frac{\mathrm{d}\tilde{z}}{\mathrm{d}\tilde{s}} = \cos\theta, \quad \frac{\mathrm{d}\tilde{S}}{\mathrm{d}\tilde{s}} = 2\pi\tilde{r}, \quad \frac{\mathrm{d}\tilde{V}}{\mathrm{d}\tilde{s}} = \pi\tilde{r}^2 \frac{\mathrm{d}\tilde{z}}{\mathrm{d}\tilde{s}}$$

$$\text{where } k = (2\pi)^{-(1/3)}, \quad \tilde{T}_\theta = \frac{T_\theta}{b_g \lambda^2}, \quad \Sigma_e = \frac{w_e g}{k b_g \lambda}$$

which is identical to Eq. (1).

Appendix B: Equations to Calculate the Heat Fluxes in the Thermal Model

The following are the equations to be used for calculating each term in Eqs. (8) and (9):

$$Q_{\text{sun}} = \alpha \cdot A_{\text{projected}} \cdot q_{sun}(1+\tau(1+r_{\text{eff}})) \tag{B1}$$

$$Q_{\text{albedo}} = \alpha \cdot A_{\text{surf}} \cdot q_{\text{albedo}}(1+\tau(1+r_{\text{eff}})) \tag{B2}$$

$$Q_{\text{IRplanet}} = \alpha_{\text{IR}} \cdot A_{\text{surf}} \cdot q_{\text{IRplanet}}(1+\tau_{\text{IR}}(1+r_{\text{effIR}})) \cdot \text{ViewFactor} \tag{B3}$$

$$Q_{\text{IRfilm}} = \sigma \cdot \varepsilon \cdot \alpha_{\text{IR}} \cdot A_{\text{surf}} \cdot T_{\text{film}}^4 (1+r_{\text{effIR}}) \tag{B4}$$

$$Q_{\text{ext}} = (T_{\text{air}} - T_{\text{film}}) \cdot A_{\text{eff}} \cdot \text{HC}_{\text{external}} \tag{B5}$$

$$Q_{\text{int}} = (T_{\text{film}} - T_{\text{gas}}) \cdot A_{\text{eff}} \cdot \text{HC}_{\text{internal}} \tag{B6}$$

$$Q_{\text{IRout}} = \sigma \cdot \varepsilon \cdot A_{\text{surf}} \cdot 2 \cdot T_{\text{film}}^4 \tag{B7}$$

Equations (B1–B7) assume that a polyethylene film is used for the balloon envelope, the planet is the Earth, and the lifting gas is helium. The bulk averaged balloon skin absorptivity of visible sunlight and IR are referred to as α and α_{IR}, respectively. The bulk averaged balloon skin emissivity of IR is denoted by ε. The bulk averaged balloon skin transmissivity of visible sunlight and IR are represented by τ and τ_{IR}, respectively. The Stephan–Boltzmann constant is represented by σ: 5.67 × 10−8 W⁄m^2 · K^4. $A_{\text{projected}}$ refers to the illuminated projected area of a balloon, which varies with solar elevation angle; and A_{surf} represents the surface area of a balloon. A_{eff} refers to the effective exposed surface area, which includes the effect of the balloon shape not fully inflated for convection. The ambient air and balloon film temperatures are

denoted by T_{air} and T_{film}, respectively. Instead of bulk averaged balloon reflectivity $r = 1 - \alpha - \tau$, the equations use the effective reflectivity $r_{\text{eff}} = r + r^2 + r^3 + \ldots$ for visible light and $r_{\text{effIR}} = r_{eff} + r_{\text{eff}}^2 + r_{\text{eff}}^3 + \ldots$ for IR.

ViewFactor is the balloon surface area diffuse-radiant view factor of the planet, which is the balloon surface area that sees the planet surface divided by the total exposed balloon surface area. Representing the radius of the Earth by R_{Earth}, which is equal to 6,371,000, the following equation is used to calculate the ViewFactor:

$$\text{ViewFactor} = \frac{1}{2}\left(1 - \cos\left(\sin^{-1}\left[\frac{R_{\text{Earth}}}{R_{\text{Earth}} + z}\right]\right)\right) \tag{B8}$$

External and internal convection heat transfer coefficients are denoted by $\text{HC}_{\text{external}}$ and $\text{HC}_{\text{internal}}$, respectively. For the external convection heat transfer coefficient, the maximum value between the free convection and the forced convection is used. The heat transfer coefficient values can be calculated using the following equations:

$$\begin{aligned} \text{HC}_{\text{free}} &= \frac{Nu_{\text{air}} \cdot k_{\text{air}}}{2r_{\max}} \\ \text{HC}_{\text{forced}} &= \frac{k_{\text{air}}}{2r_{\max}} \cdot (2 + 0.41 \cdot Re^{0.55}) \\ \text{HC}_{\text{internal}} &= 0.13 \cdot k_{\text{gas}} \cdot \left(\frac{\rho_{\text{gas}}^2 \cdot g \cdot |T_{\text{film}} - T_{\text{gas}}| \cdot Pr_{\text{gas}}}{T_{\text{gas}} \cdot \mu_{\text{air}}^2}\right)^{1/3} \end{aligned} \tag{B9}$$

Nu is the Nusselt number, and k_{gas} is the conductivity of lifting gas. The maximum radius of the balloon is $r_{\max}$, Re stands for the Reynolds number, and Pr_{gas} represents the Prandtl number for the lifting gas. In the present work, the effect of clouds in the sky is neglected, so the direct solar flux q_{sun} is equal to

the solar irradiance flux. Albedo flux at the top of the atmosphere is achieved by multiplying the albedo factor by the solar irradiance flux, where the value decreases if the solar angle is not directly overhead. Planetary diffuse infrared flux q_{IRplanet} is calculated by multiplying the infrared diffuse flux at ground level q_{IRground} by the transmissivity of the atmosphere. Finally, the following equations are needed to calculate Eqs. (B1), (B2), and (B3):

$$\begin{aligned} q_{\text{sun}} &= I_{\text{sun}} \\ q_{\text{albedo}} &= \text{Albedo} \cdot I_{\text{sun}} \cdot \sin(\text{ELV}) \\ q_{\text{IRplanet}} &= q_{\text{IRground}} \cdot \tau_{\text{atmIR}} = \varepsilon_{\text{ground}} \cdot \sigma \cdot T_{\text{ground}}^4 \cdot \tau_{\text{atmIR}} \end{aligned} \tag{B10}$$

References

[1] Jones, W. V., “Evolution of Scientific Ballooning and its Impact on Astrophysics Research,” Advances in Space Research, Vol. 53, No. 10, 2014, pp. 1405–1414.
doi:10.1016/j.asr.2013.12.028

[2] Russo, G., Carmicino, C., de Matteis, P., Marini, M., Rufolo, G., Di Palma, L., Belardo, M., Corraro, F., and Verde, L., “Unmanned Space Vehicle Program: DTFT in Flight Experiments,” 18th ESA Symposium on European Rocket and Balloon Programmes and Related Research, 2007, pp. 89–96.

[3] Yamada, K., Abe, T., Suzuki, K., Honma, N., Koyama, M., Nagata, Y., Abe, D., Kimura, Y., Hayashi, A. K., Akita, D., and Makino, H., “Deployment and Flight Test of Inflatable Membrane Aeroshell Using Large Scientific Balloon,” AIAA Paper 2011-2579, 2011.

[4] Katikala, S., “GOOGLE™ PROJECT LOON,” InSight: Rivier Academic Journal, Vol. 10, No. 2, 2014.

[5] Randolph, T. M., Mullenax, R., Schwantes, C., Sell, S.W., and Ball, D. R., “The First Balloon Flight of the Low Density Supersonic Decelerator Technology Demonstration Mission,” 2015 IEEE Aerospace Conference, IEEE, Piscataway, NJ, 2015, pp. 1–12.

[6] Farley, R., “BalloonAscent: 3-D Simulation Tool for the Ascent and Float of High-Altitude Balloons,” AIAA Paper 2005-7412, 2005.

[7] Garde, G. J., “Comparison of Two Balloon Flight Simulation Programs,” AIAA 5th Aviation, Technology, Integration and Operations Conference

(ATIO), AIAA Paper 2005-7413, 2005.

[8] Palumbo, R., Russo, M., Filippone, E., and Corraro, F., "ACHAB: Analysis Code for High-Altitude Balloons," AIAA Atmospheric Flight Mechanics Conference and Exhibit, AIAA Paper 2007-6642, 2007.

[9] Van Dosselaer, I., "Buoyant Aerobot Design and Simulation Study: BADS," Ph.D. Dissertation, Delft Univ. of Technology, Delft, The Netherlands, 2014.

[10] Palumbo, R., Morani, G., and Corraro, F., "Effective Approach to Characterization of Prediction Errors for Balloon Ascent Trajectories," Journal of Aircraft, Vol. 47, No. 4, 2010, pp. 1331–1337.
doi:10.2514/1.47005

[11] Sóbester, A., Czerski, H., Zapponi, N., and Castro, I., "High-Altitude Gas Balloon Trajectory Prediction: A Monte Carlo Model," AIAA Journal, Vol. 52, No. 4, 2014, pp. 832–842.
doi:10.2514/1.J052900

[12] Dai, Q., Fang, X., Li, X., and Tian, L., "Performance Simulation of High Altitude Scientific Balloons," Advances in Space Research, Vol. 49, No. 6, 2012, pp. 1045–1052.
doi:10.1016/j.asr.2011.12.026

[13] Zhang, Y., and Liu, D., "Influences of Initial Launch Conditions on Flight Performance of High Altitude Balloon Ascending Process," Advances in Space Research, Vol. 56, No. 4, 2015, pp. 605–618.
doi:10.1016/j.asr.2015.04.031

[14] Yajima, N., Imamura, T., Izutsu, N., and Abe, T., Scientific Ballooning, Springer, Berlin, 2004.

[15] Palumbo, R., “A Simulation Model for Trajectory Forecast, Performance Analysis and Aerospace Mission Planning with High Altitude Zero Pressure Balloons,” Ph.D. Dissertation, University of Naples “Federico II,” Naples, Italy, 2008.

[16] Conrad, G., and Robbins, E., “Determination of Balloon Drag,” AIAA International Balloon Technology Conference, AIAA Paper 1991-3666, 1991.